Contents lists available at GrowingScience

Engineering Solid Mechanics

homepage: www.GrowingScience.com/esm

Thermoelastic medium with swelling porous structure and impedance boundary under dual-phase lag

Rajneesh Kumar[a], Divya Batra[b*] and Saurav Sharma[c]

[a]*Department of Mathematics, Kurukshetra University, Kurukshetra, India, 136119*
[b]*Department of Mathematics, Kishan Lal Public College, Rewari, India, 123401*
[c]*Department of Industrial Engineering, University of Houston, Houston, United States*

A R T I C L E I N F O

Article history:
Received 10 April 2024
Accepted 2 August 2024
Available online
3 August 2024

Keywords:
Dual phase latency
Amplitude ratios
Energy ratios
Swelling porous
Reflection

A B S T R A C T

This paper investigates the impact of dual phase latency caused by the reflection of plane waves that propagate in a swelling porous thermoelastic medium with an impedance boundary. Two transversal waves (*SVS*, *SVF*), a thermal wave (*T*), and two longitudinal waves (*Ps* and *Pf*) propagate with distinct velocities. Reflection coefficients are determined by the incidence of these waves, and energy ratios for reflected waves are calculated and illustrated using these amplitude ratios. In this particular instance, the current model was downsized to an LS model. It has been noted that the energy ratios acquired are significantly influenced by dual phase lag. The results that have been obtained may be beneficial in a variety of engineering problems that are related to structure.

1. Introduction

The theory of thermoselasticity, which is characterized by a finite speed for thermal signals, has garnered significant attention in recent decades as a result of its potential relevance in the area of aerodynamic engineering and seismology. Lord and Shulman (1967) replaced the classical Fourier's law with a new wave type heat equation, which is also referred to as LS theory or extended thermoelastic theory. They employed only one thermal relaxation time. The microstructural interface effect is associated with the dual-phase lag model (DPL) in the rapid temporary heat process. Chandrasekharaiah (1998) was the first to introduce the dual phase lag model in the theory of thermos elasticity. Ramadan and AL-Nimr (2009) employed a dual phase lag model to investigate the reflection and transmission phenomena of thermal waves in a two-layer slab with imperfect contact. Their findings indicated that the thermal contact resistance should be minimized in order to mitigate thermal stress. Abouelregal (2011) examined the influence of dual-phase lag parameters on the reflection of P and SV waves from magneto-thermoelastic solid half space. He found that the reflection coefficients are considerably affected by the magnetic field, but the thermal coupling parameter has the least impact. Singh (2012) obtained reflection coefficients as a result of the motion of waves in a dual-phase lag anisotropic thermoelastic solid half-space. Kumar (2012) investigated the reflection of plane waves in thermodiffusive elastic half-space with cavities. Sharma *et al.* (2013) explored the impact of micropolar thermoelastic solid with two temperatures on wave propagation, which is surrounded by strata of half spaces of inviscid liquid. Zenkour et al. (2013) have observed that dual phase lag has a more significant impact on the reflection of thermoelastic waves from isothermal and stress-free and boundaries than other thermoelastic theories.

Sharma *et al.* (2013, 2014) considered the reflection and refraction of plane waves in micropolar elastic solids. The uniqueness and reciprocal theorems for dual-phase lag thermoelastic theory were established by El-Karamany and Ezzat (2014) through the use of Laplace transformation. Kumar and Gupta (2015) proposed a dual phase lag diffusion model and augmented classical Fick law to investigate the reflection and refraction of waves at the boundary of thermoelastic and elastic diffusion media. Alla *et al.* (2016) employed a dual phase lag model to derive the expression of amplitude ratios resulting from the reflection of waves from the electro-magnetic thermoelastic half space. They then compared the results to those of

* Corresponding author.
E-mail addresses: divyabatra1982@gmail.com (D. Batra)

ISSN 2291-8752 (Online) - ISSN 2291-8744 (Print)

doi: 10.5267/j.esm.2024.8.001

the LS theory. In the context of a time differential dual phase lag thermoelastic model, Chirita (2017) established the results of continuous dependence and uniqueness.

Deswal *et al*. (2019) found that the reflection coefficients for the DPL model are modest in comparison to those of the LS theory. Kalkal *et al.* (2019) employed a dual phase lag model to analyse the impact of initial stress and fiber reinforcement on the reflection and transmission coefficients. Dahahb *et al*. (2019) conducted an investigation into the impact of gravity and rotation on an electro-magneto-thermoelastic medium. They found that the solutions derived for the LS and DPL models exhibit the same tendency along the z-axis. The non-local dual phase lag model (DPL) was introduced by Kumar *et al*. (2019) to investigate the impact of thermomass and thermoelastic properties on nan-scale heat transport. The authors concluded that the non-local dual phase lag model is more realistic than the dual phase model. Lata *et al*. (2020) analyzed the elastic properties of waves propagating in a magneto-thermoelastic medium using a dual phase lag model and obtained reflection coefficients. Kumar *et al*. (2021) performed a study on the influence of nonlocal, void, and micropolar parameters on the reflection of waves from the thermoelastic half space using a DPL model. They then compared the results to those obtained using the LS model.

Sharma and Khator (2021, 2022) investigated certain issues related to the generation of electricity from renewable sources. Sharma *et al*. (2022) investigated the impact of impedance parameters on the propagation of waves in a micropolar thermoelastic medium using a modified Green-Lindsay (GL) theory. Khan and Tanveer (2022) employ a dual phase latency model to determine the reflection and transmission coefficient of SV waves that are propagating at the solid-liquid interface. Kumar *et al*. (2023) investigated the influence of non-local dual phase latency and double porosity on the propagation of waves at the boundary of a double porous thermoelastic medium and an inviscid liquid half-space. Ma and Liu (2023) developed a non-local thermoelastic model and discovered that the deflection parameter of the nanoplate is reduced by the nonlocal heat parameter and increased by the nonlocal structural parameter. The impact of nonlocal triclinic micropolar thermoelastic medium on the reflection and transmission of the plane wave propagating at the interface with distinct elastic properties was obtained by Kumar *et al*. (2024). Additionally, they conducted a comparison between the phase velocity and energy ratios obtained from the DPL model and the LS theory. In order to investigate the influence of hall current and initial stress on micropolar thermoelastic theory under dual phase lag, Abouelregal and Rashid (2024) employed higher order time derivatives. In their study of the sensitivity of the heating process of thin metal films, Majchrzak and Mochnacki (2024) examined that the sensitivity of the temperature field remains high when the metal has a higher mean conductivity. In a transversely isotropic exponentially graded thermoelastic medium with cavities, Barak *et al*. (2024) investigated the impact of dual phase lag and non-local lag models. Additional issues concerning the reflection of waves under dual phase latency are detailed in (Deswal *et al.*, 2024; Punia *et al.*, 2024; Eraki *et al.*; 2024).

In the current study, the reflection of plane waves from the half space of a swelling porous thermoelastic medium with impedance boundary conditions under dual phase lag is studied. There are two longitudinal waves, a thermal wave, and two transversal waves that propagate at varying speeds. The numerical computation of reflection coefficients and energy ratios resulting from the incidence of each wave. The energy ratios in dual phase lag (DP) and LS model are compared numerically and presented through a graphical representation.

2. Fundamental Equations

Fundamental equations in swelling porous thermoelastic medium when body forces are ignored is given as Eringen (1994)

$$\mu u^s_{i,jj} + (\lambda+\mu)u^s_{j,ji} - \sigma^f u^f_{j,ji} + \xi^{ff}\left(\dot{u}^f_i - \dot{u}^s_i\right) + (\gamma^f - \alpha_0)\nabla T = \rho^s_0 \ddot{u}^s_i \tag{2.1}$$

$$\mu_v \dot{u}^f_{i,jj} + (\lambda_v+\mu_v)\dot{u}^f_{j,ji} - \sigma^f u^s_{j,ji} - \sigma^{ff} u^f_{j,ji} - \xi^{ff}\left(\dot{u}^f_i - \dot{u}^s_i\right) - (\gamma^f + \alpha^f)\nabla T = \rho^f_0 \ddot{u}^f_i \tag{2.2}$$

$$K^*\left(1+\tau_T\frac{\partial}{\partial t}\right)\nabla^2 T = \left(1+\tau_q\frac{\partial}{\partial t}+\frac{{\tau_q}^2}{2!}\frac{\partial^2}{\partial t^2}\right)\left(T_0\alpha^f\nabla.\dot{u}^f + \alpha_0 T_0\nabla.\dot{u}^s + \alpha_1 T_0\dot{T}\right) + \zeta^f\left(\nabla.\dot{u}^f + \nabla.\dot{u}^s\right) \tag{2.3}$$

$$t^s_{ij} = \left(-\alpha_0 T - \sigma^f u^f_{r,r} + \lambda u^s_{r,r}\right)\delta_{ij} + \mu(u^s_{i,j} + u^s_{j,i}) \tag{2.4}$$

$$t^f_{ij} = \left(-\alpha^f T - \sigma^f u^s_{r,r} - \sigma^{ff}\nabla.u^f + \lambda_v \dot{u}^f_{r,r}\right)\delta_{ij} + \mu_v(u^f_{i,j} + u^f_{j,i}) \tag{2.5}$$

2.1 Nomenclature

λ, μ	=	lame's parameters (N/m^2)
ρ^s_0, ρ^f_0	=	mass density in solid and fluid in natural state (Ns^2/m^4)
σ^f, σ^{ff}	=	dissipation constant (N/m^2)
ξ^{ff}	=	coupling coefficient (Ns/m^4)
λ_v, μ_v	=	viscosity coefficient (Ns/m^2)
T	=	temperature (K)

T_0	=	uniform temperature (K)
K^*	=	thermal conductivity (N/sK)
$\alpha^f, \alpha_0, \gamma^f$	=	material constants (N/m^2K)
α_1	=	material constant (N/m^2K^2)
τ_T	=	phase lag parameter of temperature gradient (s)
τ_q	=	phase lag parameter of heat flux (s)
ζ^f	=	material constant related to liquid (N/m^2)
t	=	time (s)
u^s, u^f	=	displacement in solid and liquid (m)
t_{ij}^s, t_{ij}^f	=	components of stress tensor in solid and liquid (N/m^2)
ω	=	angular frequency(rad/s)
k	=	wave number (m^{-1})
z_1, z_2, z_3, z_4	=	impedance parameters (Ns/m^3)
z_5	=	impedance parameter (N/mK)
δ_{ij}	=	Kronecker delta function (dimensionless)

3. Problem formation and resolution

A homogeneous, isotropic swelling porous thermoelastic half-space has been taken into account. The origin of the rectangular cartesian coordinate system (x_1, x_2, x_3) is located at the boundary $x_3 = 0$, with the x_3-axis pointing ordinarily into the medium. The intersection of the plane wavefront and the plane surface is represented by the x_2-axis. We limit our analysis to the plane strain problem that is parallel to the $x_1 - x_3$ plane. We employ the following approach for two-dimensional problems:

$$u^k = (u_1^k, 0, u_3^k)\ ;\ k=s,f \tag{3.1}$$

Define dimensionless quantities as:

$$x_i' = \frac{\omega^*}{c_1}x_i, u_i^{k\prime} = \frac{\rho_0^s\omega^* c_1}{\alpha_0 T_0}u_i^k, t_{ij}^{k\prime} = \frac{t_{ij}^k}{\alpha_0 T_0}, T' = \frac{T}{T_0}, t' = \omega^* t, \tau_T{}' = \omega^*\tau_T, \tau_q{}' = \omega^*\tau_q, \omega' = \frac{\omega}{\omega^*}, \tag{3.2}$$

$$z_l' = \frac{z_l}{\rho_0^s c_1}, z_5' = \frac{c_1}{K^*}z_5$$

where $\omega^* = \frac{\alpha_1 T_0 c_1^2}{K^*}, c_1^2 = \frac{\lambda + 2\mu}{\rho_0^s}$ $\qquad$ $k=s,f;\ i,j=1,2,3, l=1,2,3,4$

The potentials ϕ and ψ are related to the displacement components $u_1^k(x_1, x_3, t)$, and $u_3^k(x_1, x_3, t)$ using the Helmholtz decomposition.

$$u_1^k = \frac{\partial\phi^k}{\partial x_1} - \frac{\partial\psi^k}{\partial x_3},\ u_3^k = \frac{\partial\phi^k}{\partial x_3} + \frac{\partial\psi^k}{\partial x_1} \tag{3.3}$$

Eqs. (2.1-2.3) with the help of Eqs. (3.1-3.3) becomes

$$\left(\nabla^2 - a_2\frac{\partial}{\partial t} - \frac{\partial^2}{\partial t^2}\right)\phi^s + \left(-a_1\nabla^2 + a_2\frac{\partial}{\partial t}\right)\phi^f - a_3 T = 0 \tag{3.4}$$

$$\left(-\delta_1^2\nabla^2 + a_2\frac{\partial}{\partial t} + \frac{\partial^2}{\partial t^2}\right)\psi^s - a_2\frac{\partial}{\partial t}\psi^f = 0 \tag{3.5}$$

$$\left(-h_1\nabla^2 + h_3\frac{\partial}{\partial t}\right)\phi^s + \left(\frac{\partial}{\partial t}\nabla^2 - h_2\nabla^2 - h_3\frac{\partial}{\partial t} - h_5\frac{\partial^2}{\partial t^2}\right)\phi^f - h_4 T = 0 \tag{3.6}$$

$$\left(-h_3\frac{\partial}{\partial t}\right)\psi^s + \left(-\delta_2^2\nabla^2\frac{\partial}{\partial t} + h_3\frac{\partial}{\partial t} + h_5\frac{\partial^2}{\partial t^2}\right)\psi^f = 0 \tag{3.7}$$

$$(d_3 i\omega)\phi^s + (d_4 i\omega)\phi^f + (d_2 + d_5\nabla^2)T = 0 \tag{3.8}$$

where

$$\delta_1^2 = \frac{\mu}{\lambda + 2\mu}, a_1 = \frac{\sigma^f}{\lambda + 2\mu}, a_2 = \frac{\xi^{ff}}{\rho_0^s\omega^*}, a_4 = \frac{\lambda}{\lambda + 2\mu}, a_3 = (1 - \tau_r), \tau_r = \frac{\gamma^f}{\alpha_0},$$

$$\delta_2^2 = \frac{\mu_v}{\lambda_v + 2\mu_v}, h_1 = \frac{\sigma^f}{\omega^*(\lambda_v + 2\mu_v)}, h_2 = \frac{\sigma^{ff}}{\omega^*(\lambda_v + 2\mu_v)}, h_3 = \frac{\xi^{ff} c_1^2}{\omega^{*2}(\lambda_v + 2\mu_v)},$$

$$h_4 = \frac{(1+\tau_1)\alpha^f \rho_0^s c_1^2}{\omega^* \alpha_0(\lambda_v + 2\mu_v)}, h_5 = \frac{\rho_0^f c_1^2}{\omega^*(\lambda_v + 2\mu_v)}, \tau_1 = \frac{\gamma^f}{\alpha^f}, b_1 = \frac{\alpha_0 \zeta^f}{\alpha_1 T_0(\lambda + 2\mu)}, \tau_2 = \frac{\alpha^f}{\alpha_0}$$

$$b_2 = \frac{\alpha_0 \alpha^f}{\alpha_1(\lambda + 2\mu)}, b_3 = \frac{\alpha_0^2}{\alpha_1(\lambda + 2\mu)}, e_1 = \frac{\sigma^{ff}}{\lambda + 2\mu}, e_2 = \frac{\lambda_v \omega^*}{\lambda + 2\mu}, e_3 = \frac{\mu_v}{\lambda + 2\mu},$$

$$d_1 = 1 - \tau_q i\omega - \frac{{\tau_q}^2}{2!}\omega^2, d_2 = 1 - \tau_T i\omega\,, d_3 = d_1 b_3 + b_1, d_4 = d_1 b_2 + b_1, d_5 = \frac{-id_1}{\omega}$$

$$\nabla^2 = \left(\frac{\partial^2}{\partial x_1^2} + \frac{\partial^2}{\partial x_3^2}\right)$$

We presume that the motion is time-harmonic and that

$$(\phi^s, \phi^f, T, \psi^s, \psi^f) = (\bar{\phi}^s, \bar{\phi}^f, \bar{T}, \bar{\psi}^s, \bar{\psi}^f) e^{i\{k(x_1 sin\theta - x_3 cos\theta) - \omega t\}} \tag{3.9}$$

where θ is the angle of inclination, k is wave number

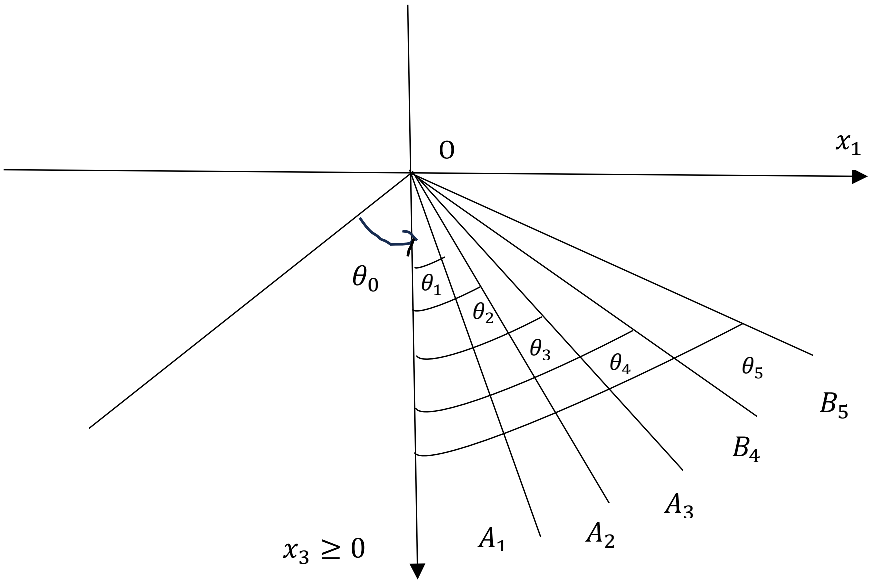

Fig. 1. Geometry of the problem depicting incident and reflected waves in swelling porous thermoelastic half-space

Using Eq. (3.9) in Eqs. (3.4) -(3.8), we can calculate the following:

$$Av^6 + Bv^4 + Cv^2 + D = 0 \tag{3.10}$$

$$A_1 v^4 + B_1 v^2 + C_1 = 0 \tag{3.11}$$

where the roots of Eq. (3.10) correspond to the velocity of the *Ps*-wave, *Pf*-wave, and *T*-wave, while the roots of Eq. (3.11) give the velocity of the *SVS*-wave and *SVF*-wave.

$A = \tau_{11} l_2 + \tau_{14} l_4, B = -l_2 \tau_{24} + l_1 \tau_{11} - a_1 l_4 + l_3 \tau_{14} - \frac{a_3}{\omega^2} l_6,, D = -\tau_{12} d_2 - a_1 h_1 d_2,$
$C = -l_1 + d_2 \tau_{11} \tau_{12} - a_1 l_3 + h_1 d_2 \tau_{14} - \frac{a_3}{\omega^2} l_5, A_1 = \tau_{11} \tau_{16} - \tau_{15} \tau_{14}, B_1 = \tau_{11} \delta_2^2 i\omega - \tau_{16} \delta_1^2, C_1 = -\delta_1^2 \delta_2^2 i\omega, \tau_{12} = i\omega + h_2, \tau_{13} = \tau_{15} + h_5, \tau_{14} = \frac{ia_2}{\omega}, \tau_{11} = 1 + \tau_{14}, \tau_{15} = \frac{ih_3}{\omega},$

$\tau_{16} = \tau_{15} - h_5, l_1 = \tau_{12} d_5 + \tau_{13} d_2 + \frac{id_4 h_4}{\omega}, l_2 = \tau_{13} d_5, l_3 = h_1 d_5 - \tau_{15} d_2 + \frac{id_3 h_4}{\omega},$

$l_4 = -\tau_{15} d_5, l_5 = (h_1 d_4 - \tau_{12} d_3) i\omega, l_6 = -(\tau_{15} d_4 + \tau_{13} d_3) i\omega$

Making use of Eqs. (3.1-3.3) in Eqs. (2.4-2.5) we obtain

$$t_{33}^{s} = -a_1\left(\frac{\partial^2\phi^f}{\partial x_1^2}+\frac{\partial^2\phi^f}{\partial x_3^2}\right)+a_4\left(\frac{\partial^2\phi^s}{\partial x_1^2}+\frac{\partial^2\phi^s}{\partial x_3^2}\right)+2\delta_1^2\left(\frac{\partial^2\phi^s}{\partial x_3^2}+\frac{\partial^2\psi^s}{\partial x_3\partial x_1}\right)-T \tag{3.12}$$

$$t_{31}^{s} = \delta_1^2\left(2\frac{\partial^2\phi^s}{\partial x_3\partial x_1}+\frac{\partial^2\psi^s}{\partial x_1^2}-\frac{\partial^2\psi^s}{\partial x_3^2}\right) \tag{3.13}$$

$$t_{33}^{f} = -a_1\left(\frac{\partial^2\phi^s}{\partial x_1^2}+\frac{\partial^2\phi^s}{\partial x_3^2}\right)-e_1\left(\frac{\partial^2\phi^f}{\partial x_1^2}+\frac{\partial^2\phi^f}{\partial x_3^2}\right)+e_2\left(\frac{\partial^2\dot\phi^f}{\partial x_1^2}+\frac{\partial^2\dot\phi^f}{\partial x_3^2}\right)+2e_3\omega^*\left(\frac{\partial^2\dot\phi^f}{\partial x_3^2}+\frac{\partial^2\dot\psi^f}{\partial x_3\partial x_1}\right)-\tau_2T \tag{3.14}$$

$$t_{31}^{f} = e_3\omega^*\left(2\frac{\partial^2\dot\phi^f}{\partial x_3\partial x_1}+\frac{\partial^2\dot\psi^f}{\partial x_1^2}-\frac{\partial^2\dot\psi^f}{\partial x_3^2}\right) \tag{3.15}$$

4. Boundary Conditions

The boundary conditions at surface $x_3 = 0$ are

(i) $t_{33}^s+\omega z_1u_3^s=0$ (ii) $t_{31}^s+\omega z_2u_1^s=0$ (iii) $t_{33}^f+\omega z_3u_3^f=0$ (4.1)
(iv) $t_{31}^f+\omega z_4u_1^f=0$ (v) $K^*\frac{\partial T}{\partial x_3}+\omega z_5T=0$

where z_1, z_2, z_3, z_4 are impedance parameters having dimension $\frac{Ns}{m^3}$. z_5 is impedance parameter having dimension $\frac{N}{mK}$. We assume the values of $\phi^s, \phi^f, T, \psi^s, \psi^f$ as:

$$\phi^s = \sum A_{0m}e^{i\{k(x_1sin\theta_0-x_3cos\theta_0)-\omega t\}}+A_me^{i\{k(x_1sin\theta_m+x_3cos\theta_m)-\omega t\}} \tag{4.2}$$

$$\phi^f = \sum \alpha_m(A_{0m}e^{i\{k(x_1sin\theta_0-x_3cos\theta_0)-\omega t\}}+A_me^{i\{k(x_1sin\theta_m+x_3cos\theta_m)-\omega t\}}) \tag{4.3}$$

$$T = \sum \beta_m(A_{0m}e^{i\{k(x_1sin\theta_0-x_3cos\theta_0)-\omega t\}}+A_me^{i\{k(x_1sin\theta_m+x_3cos\theta_m)-\omega t\}}) \tag{4.4}$$

$$\psi^s = \sum B_{0n}e^{i\{k(x_1sin\theta_0-x_3cos\theta_0)-\omega t\}}+B_ne^{i\{k(x_1sin\theta_n+x_3cos\theta_n)-\omega t\}} \tag{4.5}$$

$$\psi^f = \sum \gamma_n(B_{0n}e^{i\{k(x_1sin\theta_0-x_3cos\theta_0)-\omega t\}}+B_ne^{i\{k(x_1sin\theta_n+x_3cos\theta_n)-\omega t\}}) \tag{4.6}$$

where $\alpha_m = \frac{\left(\frac{h_4}{\omega^2}\right)V^2(-1+\tau_{11}V^2)-\left(\frac{a_3}{\omega^2}\right)V^2(h_1-\tau_{15}V^2)}{(a_1-\tau_{14}V^2)\left(\frac{-h_4}{\omega^2}\right)V^2+\left(\frac{a_3}{\omega^2}\right)V^2(\tau_{12}+\tau_{13}V^2)}$,

$\beta_m = \frac{(-1+\tau_{11}V^2)(\tau_{12}+\tau_{13}V^2)-(a_1-\tau_{14}V^2)(h_1-\tau_{15}V^2)}{(a_1-\tau_{14}V^2)\left(\frac{-h_4}{\omega^2}\right)V^2+\left(\frac{a_3}{\omega^2}\right)V^2(\tau_{12}+\tau_{13}V^2)}$, $\gamma_n = \frac{\delta_1^2-\tau_{11}V^2}{-\tau_{14}V^2}$ *(m=1,2,3; n=3,4)*

where $A_{0m}(m=1,2,3)$ denote amplitude of incident *Ps*-wave, *Pf*-wave and *T*-wave $A_m(m=1,2,3)$correspond to reflected *Ps*-wave, *Pf*-wave and *T*-wave, $B_{0n}(n=3,4)$ signify amplitude of incident *SVS*-wave and *SVF*-wave and $B_n(n=3,4)$ associate with the reflected *SVS*-wave and *SVF*-wave.

Snell's Law is denoted as $\frac{sin\theta_0}{v_0} = \frac{sin\theta_i}{v_i}$ *(i=1,2,3,4,5)*

where $k_1v_1 = k_2v_2 = k_3v_3 = k_4v_4 = k_5v_5 = \omega$

The following relation coefficients (or amplitude ratios) are obtained by applying boundary conditions (4.1) to Eq. (3.3), Eqs. (3.12-3.15).

$$\sum a_{pj}Z_j = g_p, \ (p,j=1,2,3,4,5) \tag{4.7}$$

$$a_{1i} = \left(\alpha_ia_1-a_4-2\delta_1^2\left(1-\left(\frac{v_i}{v_1}\right)^2sin^2\theta_0\right)-\frac{\beta_i}{k_i^2}\right)\left(\frac{v_1}{v_i}\right)^2+\frac{v_1^2}{v_i}z_1\sqrt{1-\left(\frac{v_i}{v_1}\right)^2sin^2\theta_0}$$

$$g_1 = (-\alpha_1a_1+a_4+2\delta_1^2cos^2\theta_0)+\frac{\beta_1}{k_1^2}+v_1z_1icos\theta_0$$

$$a_{1j} = -2\delta_1^2 sin\theta_0 \sqrt{1-\left(\frac{v_j}{v_1}\right)^2 sin^2\theta_0}\left(\frac{v_1}{v_j}\right) + iz_1 v_1 sin\theta_0$$

$$a_{2i} = -2\delta_1^2 sin\theta_0 \sqrt{1-\left(\frac{v_j}{v_1}\right)^2 sin^2\theta_0}\left(\frac{v_1}{v_i}\right) + iz_2 v_1 sin\theta_0$$

$$a_{2j} = \delta_1^2\left(-\left(\frac{v_j}{v_1}\right)^2 sin^2\theta_0 + \left(1-\left(\frac{v_j}{v_1}\right)^2 sin^2\theta_0\right)\right)\left(\frac{v_1}{v_j}\right)^2 - \frac{v_1^2}{v_j} iz_2 \sqrt{1-\left(\frac{v_j}{v_1}\right)^2 sin^2\theta_0}$$

$$g_2 = (-2\delta_1^2 sin\theta_0 cos\theta_0) - iz_2 v_1 sin\theta_0$$

$$a_{3i} = \left(a_1 + e_1\alpha_i + ik_i v_i \alpha_i\left(e_2 + 2e_3\omega^*\left(1-\left(\frac{v_i}{v_1}\right)^2 sin^2\theta_0\right)\right) - \frac{\tau_2\beta_i}{k_i^2}\right)\left(\frac{v_1}{v_i}\right)^2 + i\alpha_i z_3 \frac{v_1^2}{v_i}\sqrt{1-\left(\frac{v_i}{v_1}\right)^2 sin^2\theta_0}$$

$$g_3 = -(a_1 + e_1\alpha_1 + ik_1 v_1 \alpha_1(e_2 + 2e_3\omega^* cos^2\theta_0)) + \frac{\tau_2\beta_i}{k_1^2} + v_1 z_3 \alpha_1 icos\theta_0$$

$$a_{3j} = ik_j\gamma_j 2e_3\omega^* v_1 sin\theta_0\sqrt{1-\left(\frac{v_j}{v_1}\right)^2 sin^2\theta_0} + iz_3\gamma_j v_1 sin\theta_0$$

$$a_{4i} = ik_i\alpha_i 2e_3\omega^* v_1 sin\theta_0\sqrt{1-\left(\frac{v_i}{v_1}\right)^2 sin^2\theta_0} + i\frac{v_1^2}{v_i} z_4\alpha_i sin\theta_0$$

$$g_4 = ik_1\alpha_1 2e_3\omega^* v_1 sin\theta_0 cos\theta_0 - iv_1 z_4 \alpha_1 sin\theta_0$$

$$a_{4j} = e_3\omega^*\left(ik_j\gamma_j v_j sin^2\theta_0 + \left(1-\left(\frac{v_j}{v_1}\right)^2 sin^2\theta_0\right)\left(-ik_j\gamma_j\frac{v_1^2}{v_j}\right)\right) - iz_4\gamma_j\frac{v_1^2}{v_j}\sqrt{1-\left(\frac{v_j}{v_1}\right)^2 sin^2\theta_0},\ g_5 = i\frac{\beta_1}{k_1}cos\theta_0 - z_5\frac{\beta_1}{k_1}v_1$$

$$a_{5i} = i\frac{\beta_i}{k_i}\left(\frac{v_1}{v_i}\right)^2\sqrt{1-\left(\frac{v_i}{v_1}\right)^2 sin^2\theta_0} + z_5\frac{\beta_i}{k_i}\frac{v_1^2}{v_i},\ ,\ a_{54} = a_{55} = 0$$

The amplitude ratios of reflected *Ps, Pf, T,* and *SVS, SVF* waves for an incident *Ps* wave are denoted by $Z_i = \frac{A_i}{A_{01}}$ *(i=1,2,3)* and $Z_j = \frac{B_j}{A_{01}}$ $(j = 4,5)$. In the same way, the amplitude ratios of reflected waves can be determined for the incident *Pf, T, SVS*, or *SVF* waves.

5. Energy ratios of reflected waves

This section calculates the dissemination of energy amongst reflected waves. In accordance with (Achenbach, 1973), the rate at which energy is transmitted per unit surface area per unit time is presented as

$$P^e = \frac{1}{2}\sum_{k=s,f}\Re((t_{33}^k)\dot{u}_3^k)) + \frac{1}{2}\sum_{k=s,f}\Re((t_{31}^k)\dot{u}_1^k)) \tag{5.1}$$

The average reflected wave energy at $x_3 = 0$ is given by

$$|E_i| = -\left(\frac{A_i}{A_{01}}\right)^2 \frac{\left(\frac{v_1}{v_i}\right)^2\sqrt{1-\left(\frac{v_i}{v_1}\right)^2 sin^2\theta_0}\left[(\alpha_i a_1 - a_4 - 2\delta_1^2) - \frac{\beta_i}{k_i^2} + r_i\right]}{cos\theta_0\left[(\alpha_1 a_1 - a_4 - 2\delta_1^2) - \frac{\beta_1}{k_1^2} + r_1\right]} \tag{5.2}$$

$$|E_j| = -\left(\frac{B_j}{A_{01}}\right)^2 \frac{\left(\frac{v_1}{v_j}\right)^2\sqrt{1-\left(\frac{v_j}{v_1}\right)^2 sin^2\theta_0}\left((-\delta_1^2 + i\omega e_3\omega^*\gamma_j^2)\right)}{cos\theta_0\left[(\alpha_1 a_1 - a_4 - 2\delta_1^2) - \frac{\beta_1}{k_1^2} + r_1\right]} \tag{5.3}$$

where, $r_i = \alpha_i(a_1 + e_1\alpha_i + ik_i\alpha_i v_i e_2 + 2ie_3\omega^* k_i\alpha_i) - \frac{\tau_2\beta_i}{k_i^2}$ *(i=1,2,3; j=4,5)*

6. Discussion and numerical outcomes

The following data is used to demonstrate the consequence of the impedance parameter on the energy ratios of reflected *Ps, Pf, T, SVS,* and *SVF* waves (Tomar & Goyal, 2013).

Symbol	Value	Unit	Symbol	Value	Unit
λ	6.0×10^{9}	N/m^2	α^f	0.152×10^{6}	$N/m^2 K$
μ	9.0×10^{9}	N/m^2	α_0	0.015×10^{6}	$N/m^2 K$
λ_v	1.002×10^{-3}	Ns/m^2	γ^f	1.656×10^{6}	$N/m^2 K$
μ_v	8.88×10^{-4}	Ns/m^2	T	298	K
σ^f	0.03×10^{6}	N/m^2	ρ_0^s	2.65×10^{3}	Ns^2/m^4
σ^{ff}	0.291×10^{5}	N/m^2	ρ_0^f	9.90×10^{2}	Ns^2/m^4
ξ^{ff}	0.0250×10^{6}	Ns/m^4	K^*	0.498×10^{2}	N/sK
α_1	0.03831×10^{2}	$N/m^2 K^2$	ζ^f	2.15×10^{6}	N/m^2

Energy ratios for reflected *Ps*-wave, *Pf*-wave, *T*-wave, *SVS*-wave, and *SVF*-wave are obtained and presented graphically in Figs. 2(a-e) to 6(a-e) using the aforementioned numerical data for $\tau_T = 0.3\ s$ and $\tau_q = 0.4\ s$ and impedance parameters $z_1 = 10$, $z_2 = 20$, $z_3 = 30$, $z_4 = 40$, $z_5 = 50$. The energy ratios $|E_p|$ $(p = 1, .., 5)$ of these waves are plotted against the angle of incidence.

7. Specific Situation

For the case in which $\tau_T = 0, \tau_q \neq 0$ and ${\tau_q}^2 = 0$ the LS-model is used to reduce the results that have been obtained.

The change in energy ratios of reflected waves in the DP (dual phase lag model) and LS model when the *Ps* wave is incident is illustrated in **Fig. 2(a-e)**. It is noted that the energy ratios of all reflected waves diminish as the angle of incidence increases. For each angle of incidence, the approximate value of E_1 remains unity for both the DP and LS models. Except for E_4, the DP model's reflected energy ratios are lower than those of the LS model.

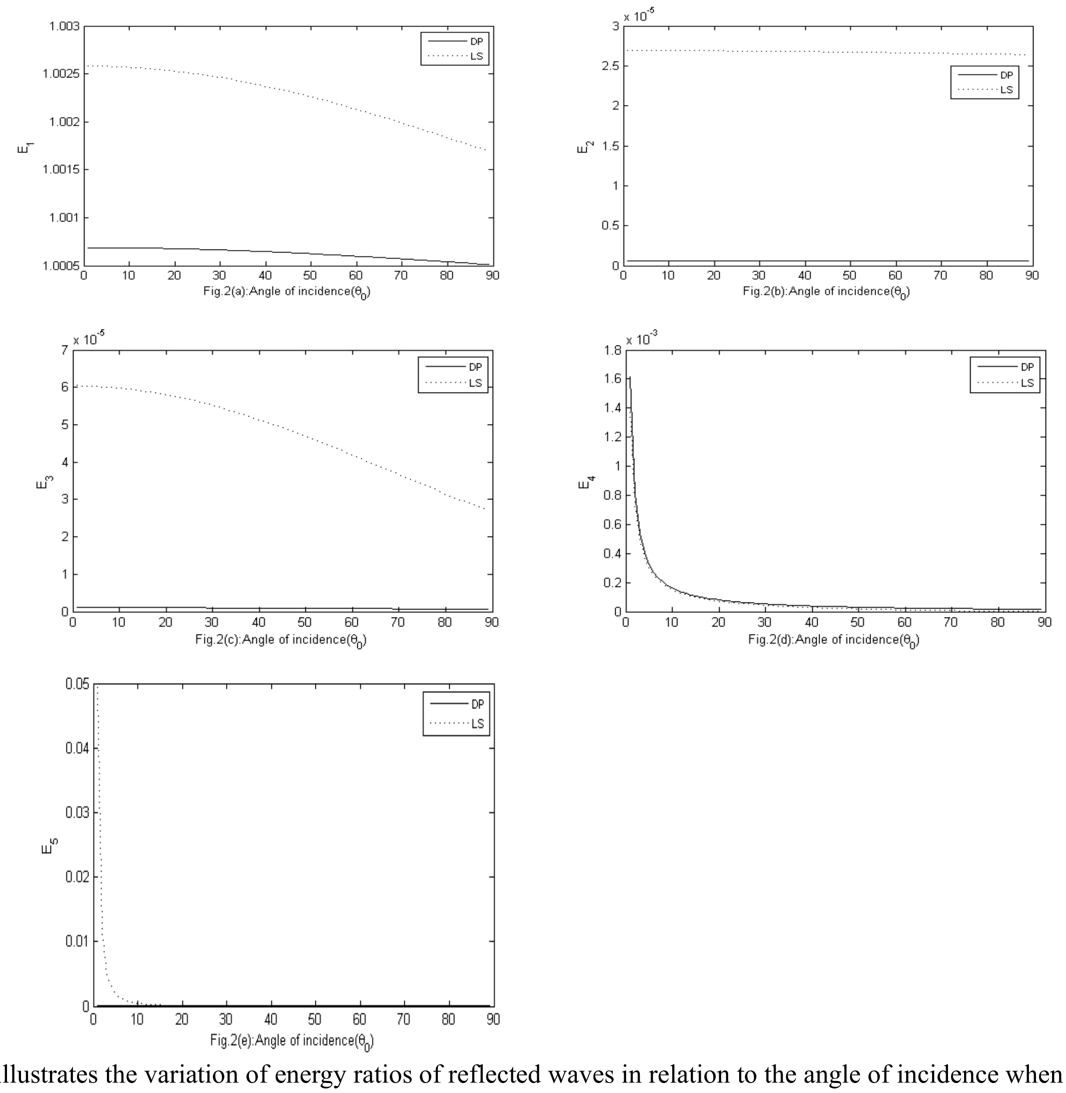

Fig. 2(a-e) illustrates the variation of energy ratios of reflected waves in relation to the angle of incidence when a *Ps* wave is incident.

Fig. 3(a-e) illustrates the reflected energy ratios that result from the incidence of the *Pf* wave. It is observed that the values of E_2, E_3, and E_4 diminish as the angle of incidence increases, while E_1 increases in both the DP and LS models. The energy ratios for E_5 initially decline and then begin to rise as the angle of incidence changes. Additionally, the initial values of E_5 for the DP model are lower than those of the LS model; however, the reverse behaviour is observed later. It is also detected that the energy ratios in the DP model are lower than those in the LS model, with the exception of E_5.

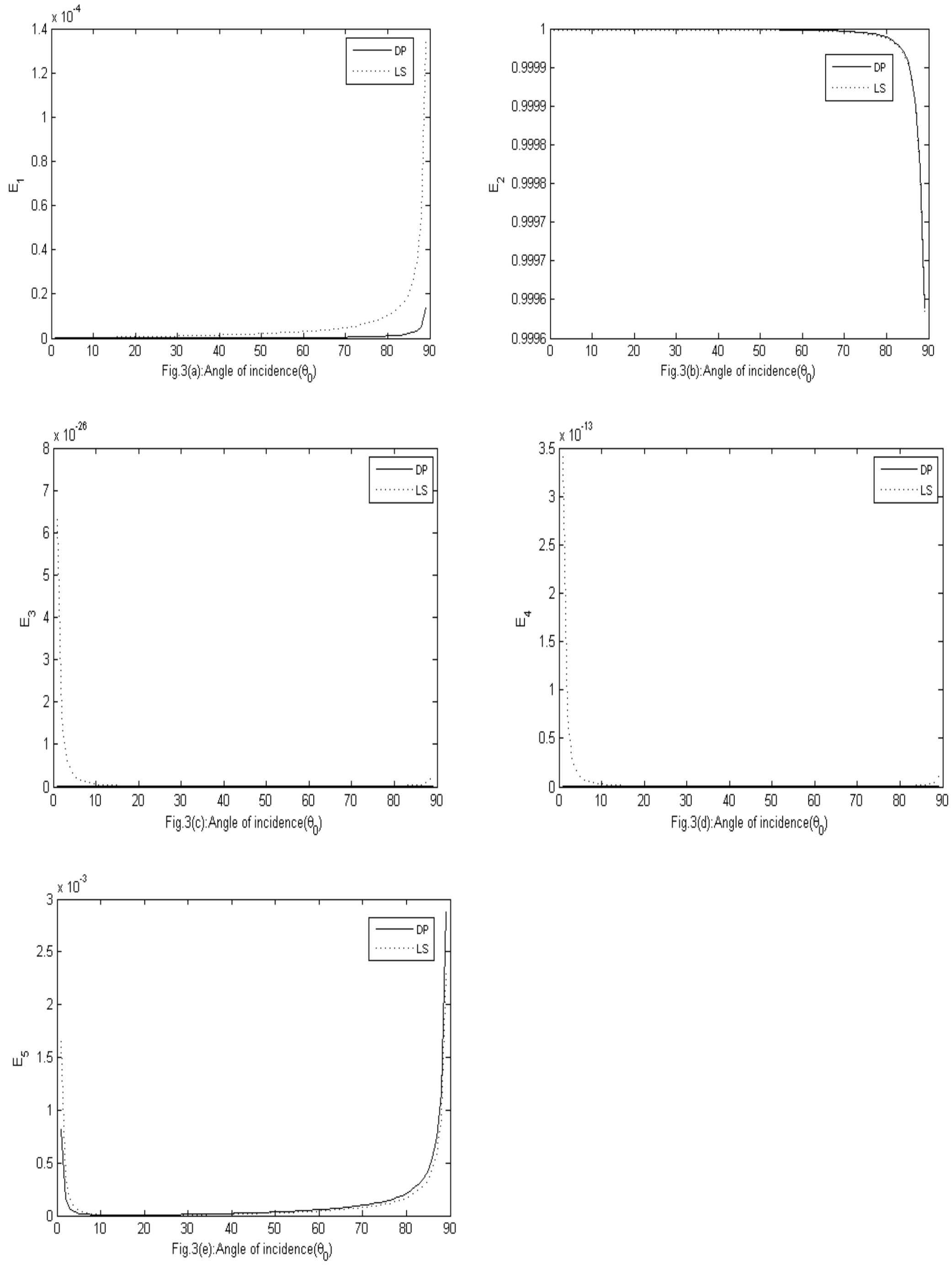

Fig. 3(a-e) illustrates the variation of energy ratios of reflected waves in relation to the angle of incidence when a *Pf* wave is incident.

Fig. 4(a-e) illustrates the variation in reflected energy ratios as a result of the incidence of the *T* wave. Energy ratios in the DP model decrease as the angle of incidence rise, with the exception of E_5. The energy ratios of the LS model exhibit oscillatory behaviour. In the DP model, energy ratios diminish as the angle of incidence changes, whereas in the LS model, they oscillate in response to the angle of incidence. The energy ratio E_2 in the LS model is lower than the results acquired for the DP model. However, the energy ratio E_3 is greater than the DP model throughout the entire spectrum.

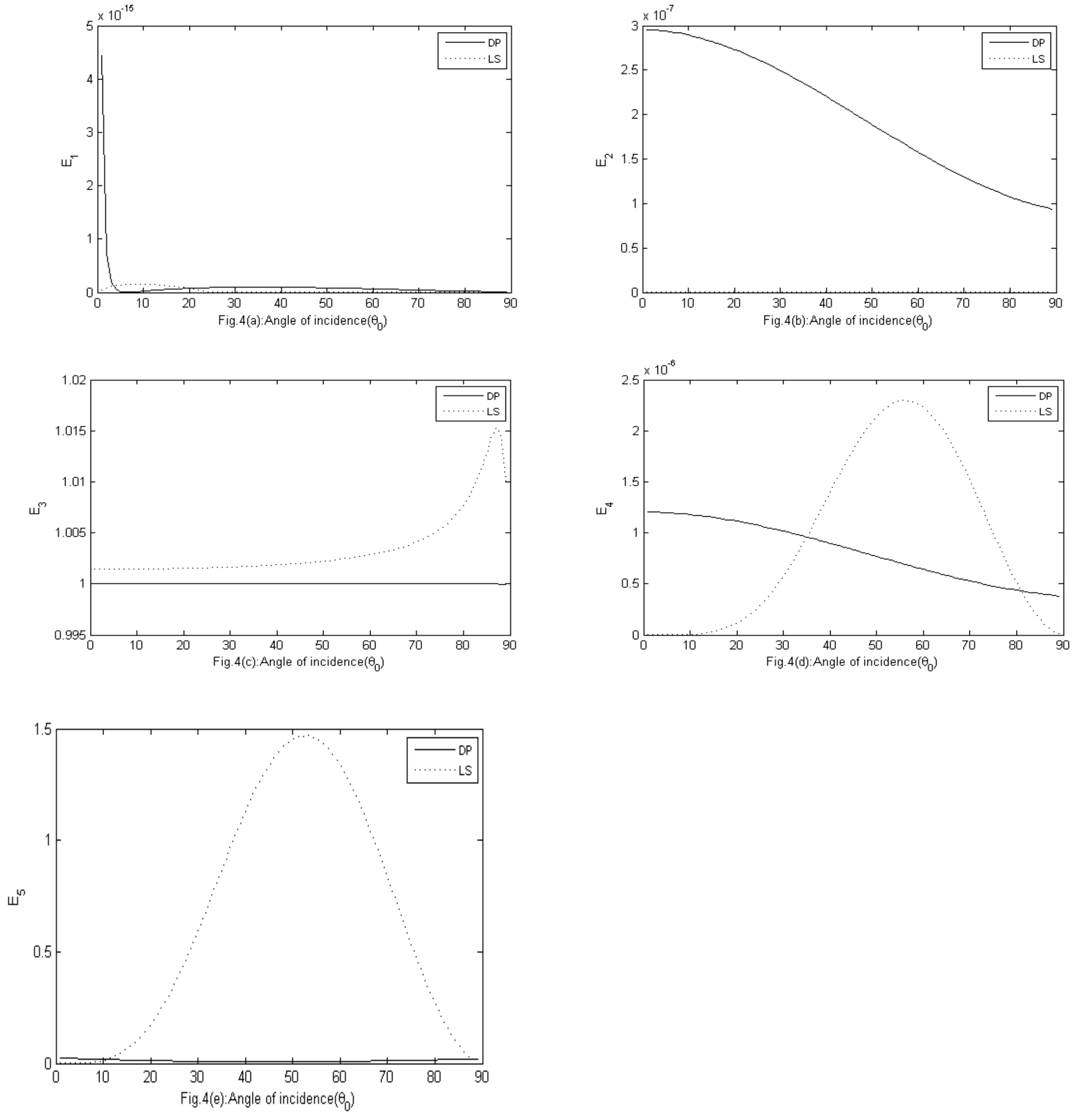

Fig. 4(a-e) illustrates the variation of energy ratios of reflected waves in relation to the angle of incidence when a *T* wave is incident.

The energy ratios of reflected waves for the DP and LS models diminish as the angle of incidence increases when the *SVS* wave is incident, as illustrated in **Fig 5(a-e).** The energy ratios in the LS model are still lower than the outcomes achieved in the DP model at each angle of occurrence. Also, the values of E_4 for both the DP and LS models decrease and converge to one.

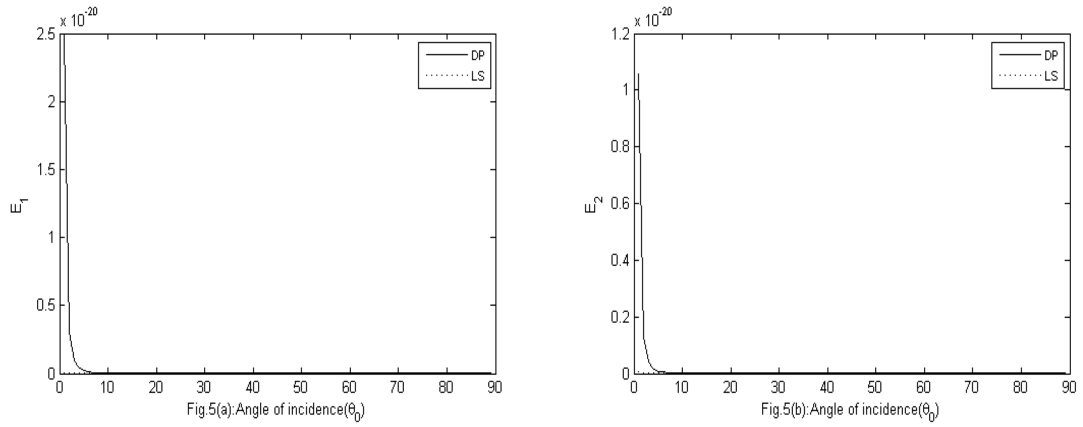

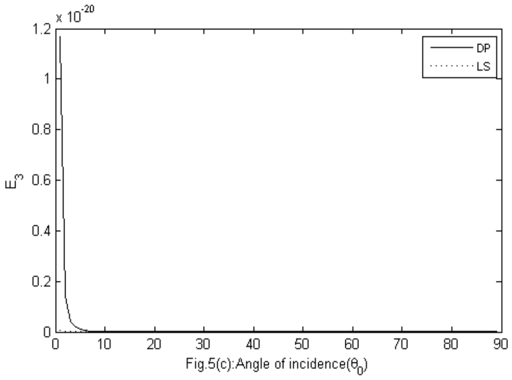

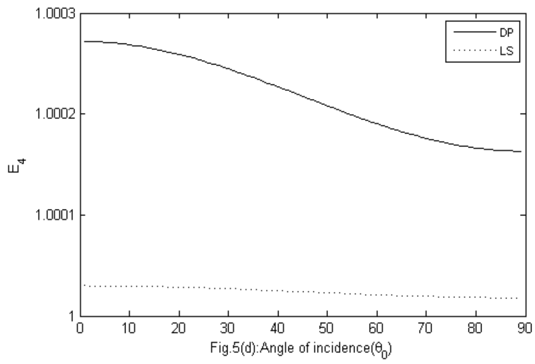

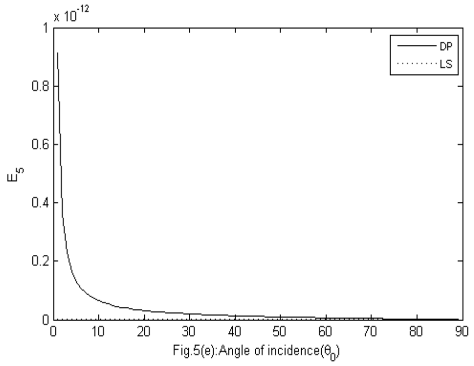

Fig. 5(a-e) illustrates the variation of energy ratios of reflected waves in relation to the angle of incidence when a *SVS* wave is incident.

The energy ratios of the reflected wave are illustrated in Fig 6(a-e) when an *SVF* wave is incident. It has been noted that the energy ratios for the DP model are higher than those obtained for the LS model. The maximal value of E_1, E_2, E_3, and E_4 is achieved at $\theta = 45^0$ in both models. The energy ratio E_5 increases with the angle of incidence, and its values remain relatively close to one at each angle of incidence.

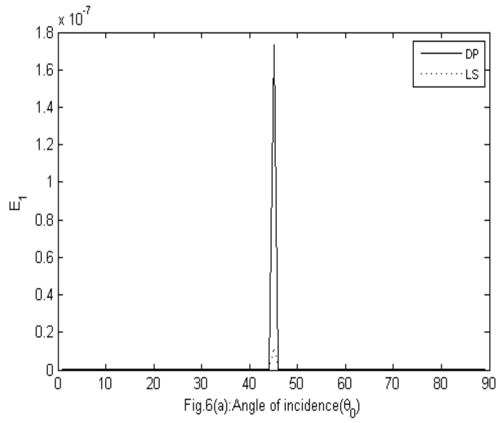

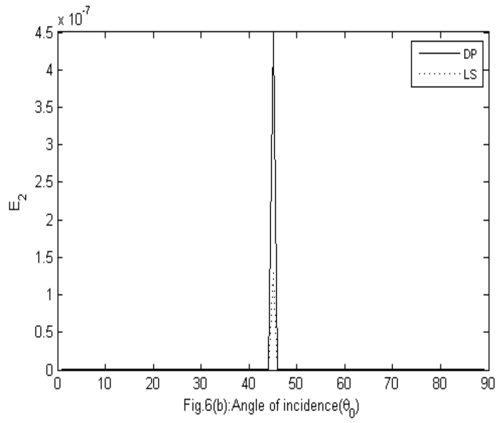

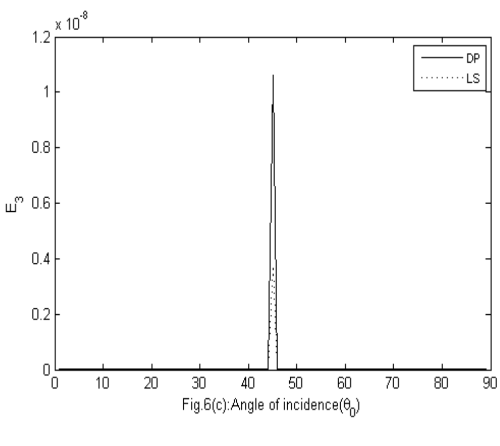

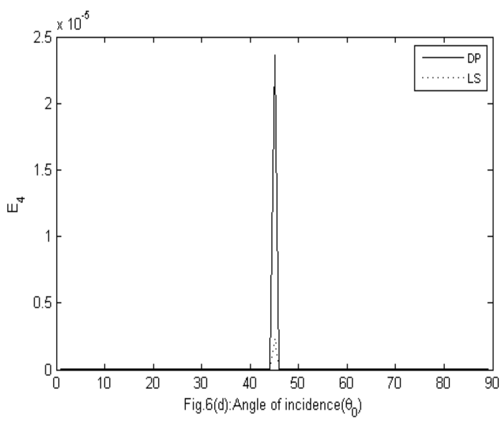

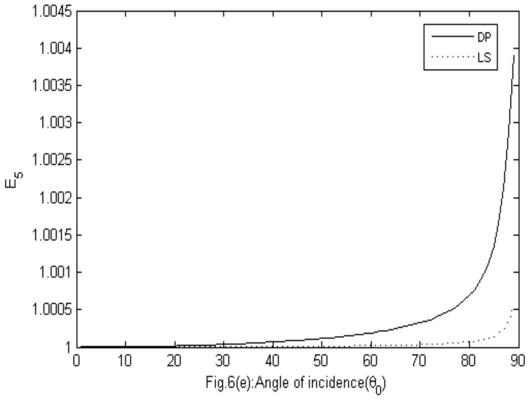

Fig. 6(a-e) illustrates the variation of energy ratios of reflected waves in relation to the angle of incidence when a *SVF* wave is incident.

8. In Conclusion

The investigation focuses on the reflection of plane waves from a porous thermoelastic medium that is enlarging and has a dual phase lag, which is subject to an impedance boundary. There are two longitudinal waves, a thermal wave, and two transversal waves. Amplitude ratios and energy ratios for the dual phase lag model and LS model are compared based on the incidence of each wave. It has been noted that the sum of the energy ratio at each angle of incidence is approximately one, which demonstrates the preservation of the law of conservation of energy. It is also detected that the energy ratios for reflected waves in the DP model are lower than the values obtained for the LS model when *Ps, Pf,* and *T* waves are incident. Conversely, the reverse behaviour is observed when transversal waves are incident. Additionally, the energy ratios reach their maximal value at $\theta = 45^0$ in both the DP and LS models when the *SVF* wave is incident. These findings may prove advantageous in the investigation of numerous seismological issues.

References

Abd-Alla, A. M., Othman, M. I., & Abo-Dahab, S. M. (2016). Reflection of Plane Waves from Electro-magneto-thermoelastic Half-space with a Dual-Phase-Lag Model. *Computers, Materials & Continua*, *51*(2).

Abouelregal, A. E. (2011). The reflection of magneto-thermoelastic P and SV waves at a solid half space using dual-phase-lag model. *Advances in Applied Mathematics and Mechanics*, *3*(6), 745-758.

Abouelregal, A. E., & Rashid, A. F. (2024). Deformation in a micropolar material under the influence of Hall current and initial stress fields in the context of a double-temperature thermoelastic theory involving phase lag and higher orders. *Acta Mechanica*, 1-27.

Achenbach J.D. (1973). *Wave propagation in elastic solids*, Ist edn. North Holland, Amsterdam.

Barak, M. S., Poonia, R., Devi, S., & Dhankhar, P. (2024). Nonlocal and dual-phase-lag effects in a transversely isotropic exponentially graded thermoelastic medium with voids. *ZAMM-Journal of Applied Mathematics and Mechanics/Zeitschrift für Angewandte Mathematik und Mechanik*, *104*(5), e202300579.

Chandrasekharaiah, D. S. (1998). Hyperbolic thermoelasticity: a review of recent literature. *Appl. Mech. Rev, 51(12)*, 705-729.

Chiriţă, S. (2017). On the time differential dual-phase-lag thermoelastic model. *Meccanica*, *52*(1), 349-361.

Deswal, S., Kalkal, K. K., Dhankhar, P., & Poonia, R. (2024). Reflection of Plane Waves in a Nonlocal Transversely Isotropic Micropolar Thermoelastic Medium with Temperature-Dependent Properties. *Journal of Vibration Engineering & Technologies*, 1-18.

Deswal, S., Sheokand, S. K., & Kalkal, K. K. (2019). Reflection at the free surface of fiber-reinforced thermoelastic rotating medium with two-temperature and phase-lag. *Applied Mathematical Modelling*, *65*, 106-119.

El-Karamany, A. S., & Ezzat, M. A. (2014). On the dual-phase-lag thermoelasticity theory. *Meccanica*, *49*, 79-89.

Eraki, E. E., Fathy, R. A., & Othman, M. I. (2024). Thomson effect on an initially stressed diffusive magneto-thermoelastic medium via dual-phase-lag model. *Journal of Vibration Engineering & Technologies*, 1-12.

Eringen, A. C. (1994). A continuum theory of swelling porous elastic soils. *International journal of engineering science*, *32*(8), 1337-1349.

Kalkal, K. K., Sheokand, S. K., & Deswal, S. (2019). Reflection and transmission between thermoelastic and initially stressed fiber-reinforced thermoelastic half-spaces under dual-phase-lag model. *Acta Mechanica*, *230*, 87-104.

Khan, A. A., & Tanveer, S. (2021). Transmission and reflection of SV waves at micropolar solid–liquid interface with dual-phase lag theory. *Indian Journal of Physics*, 1-13.

Kumar, D., Paswan, B., Singh, P., & Chattopadhyay, A. (2024). Reflection and transmission of plane wave at the interface between two distinct nonlocal triclinic micropolar generalized thermoelastic half spaces under DPL and LS theory. *Acta Mechanica*, *235*(5), 3245-3270.

Kumar, R., & Gupta, V. (2015). Dual-phase-lag model of wave propagation at the interface between elastic and thermoelastic diffusion media. *Journal of Engineering Physics and Thermophysics*, *88*, 252-265.

Kumar, R., Gupta, V., Pathania, V., Kumar, R., & Barak, M. S. (2023). Analysis of waves at boundary surfaces at distinct media with nonlocal dual-phase-lag. *Proceedings of the National Academy of Sciences, India Section A: Physical Sciences*, *93*(4), 573-585.

Kumar, R., Kaushal, S., & Kochar, A. (2022). Response of impedance parameters on waves in the micropolar thermoelastic medium under modified Green-Lindsay theory. *ZAMM-Journal of Applied Mathematics and Mechanics/Zeitschrift für Angewandte Mathematik und Mechanik*, *102*(9), e202200109.

Kumar, R., Sheoran, D., Thakran, S., & Kalkal, K. K. (2021). Waves in a nonlocal micropolar thermoelastic half-space with voids under dual-phase-lag model. *Waves in Random and Complex Media*, 1-20.

Kumar, R., Vashishth, A. K., & Ghangas, S. (2019). Nonlocal heat conduction approach in a bi-layer tissue during magnetic fluid hyperthermia with dual phase lag model. *Bio-medical materials and engineering*, *30*(4), 387-402.

Lata, P., Kaur, I., & Singh, K. (2020). Propagation of plane wave in transversely isotropic magneto-thermoelastic material with multi-dual-phase lag and two temperature. *Coupled systems mechanics*, *9*(5), 411-432.

Lord, H. W., & Shulman, Y. (1967). A generalized dynamical theory of thermoelasticity. *Journal of the Mechanics and Physics of Solids*, *15*(5), 299-309.

Ma, J., & Liu, H. (2023). Thermodynamic behavior of rectangular nanoplate under moving laser pulse based on nonlocal dual-phase-lag model. *International Journal of Heat and Mass Transfer*, *207*, 123958.

Majchrzak, E., & Mochnacki, B. (2024). Sensitivity of a Process for Heating Thin Metal Film Described by the Dual-Phase Lag Equation with Temperature-Dependent Thermophysical Parameters to Perturbations of Lag Times. *Energies*, *17*(10), 2252.

Punia, B. S., Deswal, S., Kalkal, K. K., & Othman, M. I. (2024). Reflection of plane waves in an orthotropic micropolar thermoelastic diffusive medium with two-temperature. *Indian Journal of Physics*, *98*(2), 613-628.

Ramadan, K., & Al-Nimr, M. D. A. (2009). Thermal wave reflection and transmission in a multilayer slab with imperfect contact using the dual-phase-lag model. *Heat transfer engineering*, *30*(8), 677-687.

Sharma, K. (2012). Reflection of plane waves in thermodiffusive elastic half-space with voids. *Multidiscipline Modeling in Materials and Structures*, *8*(3), 269-296.

Sharma, K., & Marin, M. (2013). Effect of distinct conductive and thermodynamic temperatures on the reflection of plane waves in micropolar elastic half-space. *University Politehnica of Bucharest Scientific Bulletin-Series A-Applied Mathematics and Physics*, *75*(2), 121-132.

Sharma, K., & Marin, M. (2014). Reflection and transmission of waves from imperfect boundary between two heat conducting micropolar thermoelastic solids. *Analele ştiinţifice ale Universităţii" Ovidius" Constanţa. Seria Matematică*, *22*(2), 151-176.

Sharma, K., Sharma, S., & Bhargava, R. R. (2013). Propagation of waves in micropolar thermoelastic solid with two temperatures bordered with layers or half spaces of inviscid liquid. *Materials Physics and Mechanics*, *16*(1), 66-81.

Sharma, S., & Khator, S. (2021). Power generation planning with reserve dispatch and weather uncertainties including penetration of renewable sources. *International Journal of Smart Grid and Clean Energy*, *10*(4), 292-303.

Sharma, S., & Khator, S. (2022). Micro-Grid Planning with Aggregator's Role in the Renewable Inclusive Prosumer Market. *Journal of Power and Energy Engineering*, *10*(4), 47-62.

Singh, B. (2013). Wave propagation in dual-phase-lag anisotropic thermoelasticity. *Continuum Mechanics and Thermodynamics*, *25*(5), 675-683.

Tomar, S. K., & Goyal, S. (2013). Elastic waves in swelling porous media. *Transport in porous media*, *100*, 39-68.

Zenkour, A. M., Mashat, D. S., & Abouelregal, A. E. (2013). The effect of dual-phase-lag model on reflection of thermoelastic waves in a solid half space with variable material properties. *Acta Mechanica Solida Sinica*, *26*(6), 659-670.